OmniScatter: Extreme Sensitivity mmWave Backscattering Using Commodity FMCW Radar

Kang Min Bae, Namjo Ahn, Yoon Chae[§],
Parth Pathak[§], Sung-Min Sohn[†], and Song Min Kim[*]
Korea Advanced Institute of Science and Technology (KAIST)
[§]George Mason University [†]Arizona State University
{bkm2259,njahn0716,songmin}@kaist.ac.kr,{ychae2,phpathak}@gmu.edu,smsohn@asu.edu

ABSTRACT

Massive connectivity is a key to the success of the Internet of Things. While mmWave backscatter has great potential, substantial signal attenuation and overwhelming ambient reflections impose significant challenges. We present `OmniScatter`, a practical mmWave backscatter with an extreme sensitivity of -115 dBm. The performance is theoretically comparable to the popular commodity RFID EPC Gen2 (900 MHz), and is empirically validated via evaluations under various practical settings with abundant ambient reflections and blockages – e.g., In an office where a tag is locked in a wooden closet 6m away, as well in libraries and retail stores where a tag is placed across two rows of metal shelves. At the heart of `OmniScatter` is the new *High Definition FMCW (HD-FMCW)*, which interplays with the tag (FSK) signal to disentangle the ambient reflections from the tag signal in the frequency domain, essentially offering immunity to ambient reflections. To further support practical deployment, `OmniScatter` offers coordination-free Frequency Division Multiple Access (FDMA) that effortlessly scales to thousands of concurrent tags. The readers were built on commodity radars and the tags were prototyped on PCB. The trace-driven evaluation demonstrates concurrent communication of 1100 tags with the BER < 1.5%, paving a pathway towards practical mmWave backscatter for everyday and anywhere use.

CCS CONCEPTS

• **Networks** → *Network range*; *Network dynamics*; **Network reliability**; **Network manageability**.

KEYWORDS

Internet-of-Things, mmWave, backscatter, retro-reflective tag, FMCW

ACM Reference Format:
Kang Min Bae, Namjo Ahn, Yoon Chae, Parth Pathak, SungMin Sohn, and Song Min Kim. 2022. OmniScatter: Extreme Sensitivity mmWave Backscattering Using Commodity FMCW Radar. In *The 20th Annual International Conference on Mobile Systems, Applications and Services (MobiSys '22), June 25–July 1, 2022, Portland, OR, USA.* ACM, New York, NY, USA, 14 pages. https://doi.org/10.1145/3498361.3538924

[*]Song Min Kim is the corresponding author (songmin@kaist.ac.kr).

MobiSys '22, June 25–July 1, 2022, Portland, OR, USA

ACM ISBN 978-1-4503-9185-6/22/06…$15.00
https://doi.org/10.1145/3498361.3538924

1 INTRODUCTION

With the Internet of Things (IoT) anticipated to grow up to a trillion devices by 2035 [53] and 6G aiming at $10/m^2$ Massive Machine-Type Communications [47], massive connectivity has long been considered a key to the success of IoT and diverse emerging services. Backscatter is an attractive option for scalability with its ultra-low power operation at tens of uW [72] offering long-term sustainability. In particular, recent advances in mmWave backscatters [7, 11, 34, 42, 52] present a great potential for scalability by exploiting the abundant spectrum resource in the mmWave ranging up to 14 GHz (60 GHz band); A bandwidth over two orders of magnitude greater than 26 MHz and 100 MHz in the popular 900 MHz and 2.4 GHz bands, respectively.

A substantial downside of mmWave is the severe signal attenuation due to the high frequency, which makes backscatter signals particularly error-prone, as they are inherently low in power. To tackle this, latest mmWave backscatter systems adopt FMCW radars – by leveraging chirp, FMCW boosts the reflected signal power in proportion to the wide mmWave bandwidth. For instance, Millimetro [52] localizes mmWave backscatters from 100m outdoors while another work [33] communicates from car to car using mmWave backscatter at 18m distance outdoors, where they use FMCW radar as a mmWave tag reader. However, such systems are designed for specific deployment scenarios, e.g., roadside for autonomous driving [52] and achieving robustness for practicality under everyday environment still remains a challenge due to the vast amount of ambient reflections (i.e., clutter noise). The signal amplification of FMCW applies equally to the rich ambient reflections from a complex environment to cause a strong self-interference against the tag signal. Our experiment in a server room (with metal racks) yields a large ambient reflect power of 37.12 dBm on average, to pull down the signal-to-noise ratios (SNR) to as low as -158.55 dB. This harsh scenario in fact introduces 44.29 dB larger noise power compared to friendly indoor/outdoor environments with less reflectors, such as hallways (57.97 dB SNR) and roadside (51.51 dB SNR). This calls for a new design that effectively mitigates the overwhelming ambient reflections in realistic and complex environments.

This paper presents `OmniScatter`, a mmWave back-scatter system with an extreme sensitivity of -115 dBm (Section 3.2), > 20 dB improvement over state-of-the-arts (-90 dBm in [42]). This stems from `OmniScatter`'s unique design that is immune to ambient reflections, while retaining the signal boost capability of the FMCW.

Systems	Coordination-free Multiplexing	NLOS Deployment	Mobility Support	Omnidirectional Comm.	Operating Bands(GHz)
OmniScatter	**Yes**	**Yes**	**Yes**	**Yes**	**24, 60**
mmTag [42]	No	No	No	No	24
mmX [41]	No	Yes	Yes	No	24
Millimetro [52]	No	Yes	Yes	No	24

Table 1: Comparison with the state-of-the-arts

We note that the sensitivity of the widely deployed 900 MHz RFID EPC Gen2 is -92 dBm [22]. As per Friis Equation, 24 GHz and 900 MHz signal strengths differ by -28.52 dB for the same distance [14]. Since OmniScatter sensitivity outperforms the 900 MHz RFID by 23 dB, OmniScatter performance is theoretically comparable to that of the RFID, indicating practicality. To demonstrate this, OmniScatter is evaluated to establish robust communication under practical and harsh scenarios with abundant reflectors and blockages, including when tags are (i) placed behind several rows of metal racks and shelves (retail stores, libraries, server rooms), (ii) enclosed in a wooden closet > 6m away from the radar (homes and offices), and (iii) packed in a cardboard box 3m away (warehouses). For further practicality, OmniScatter offers coordination-free FDMA for economic operation of OmniScatter at scale. Furthermore, OmniScatter is kept affordable by implementing the reader on commodity mmWave radars (~200 USD). The tags are kept as simple as possible for low power operation (7uW). They perform low rate (< 10 MHz) FSK modulation through effortless impedance switching, which we prototyped on a PCB. Table 1 summarizes the comparison to the state-of-the-art mmWave backscatter (or low power) systems, showcasing that OmniScatter is uniquely positioned towards practical mmWave backscatter for everyday use.

At the heart of OmniScatter is the unique reader, named *High Definition FMCW (HD-FMCW)* radar, serving as a foundation to the entire OmniScatter design. HD-FMCW is a new variant of FMCW radar exclusively designed for OmniScatter, which interplays with the tag (FSK) signal to enable extreme sensitivity and coordination-free FDMA. Specifically, HD-FMCW leverages multi-chirp symbols to effectively disentangle the ambient reflection from the tag signal in the frequency domain. This yields a vast amount of 50 dB SNR gain on top of the original FMCW, enabling tags with SNR as low as -106.05 dB to be successfully decoded (0.22% BER). This lays a solid foundation for practical mmWave backscatter. OmniScatter reveals extremely weak NLOS backscatter signals otherwise buried under excessive ambient reflections. Benefiting from the extreme sensitivity, OmniScatter operates with omni-directionality, under which all our evaluations are performed. This was implemented by only enabling a single antenna within the MIMO configuration on the commodity radar. Omni-directionality offers OmniScatter a low communication latency and the support for mobile backscatters, both of which are important aspects towards realistic scenarios with numerous tags. This was evaluated with a retro-reflective antenna (i.e., Van Atta array). HD-FMCW was implemented and evaluated on 24 GHz and 60 GHz commodity radars to ensure generality.

HD-FMCW leverages the distance-frequency relationship in the radar to passively allocate channels to the tags according to the tag-radar distance. This avoids any coordination cost and the channel switching overhead for the tags (thus coordination-free FDMA), enabling the tags to exploit the wide mmWave bandwidth without the power-hungry high-frequency local oscillators (LO) and filters [49]. Validations include a 1100-tag evaluation performed on extensive traces collected in a large lecture hall, which demonstrated < 1.5% BER for all 1100 concurrent tag communication. Lastly, OmniScatter offers a simple coverage and density configuration mechanism by adjusting HD-FMCW settings. To summarize, the contributions are three-fold:

- We design OmniScatter, which uniquely and collectively brings a combination of extreme sensitivity and coordination-free deployment for practical mmWave backscattering in the wild.
- OmniScatter's novel HD-FMCW radar effectively disentangles the FSK tag signal from clutter noise to reach -115 dBm sensitivity. This serves as a foundational technique for robust mmWave backscatter communication and effective utilization of the mmWave bandwidth in a passive manner.
- We implement readers using commodity mmWave radars [13, 23, 58] and the tags were prototyped on PCB (24 GHz) and commodity RF switches (60 GHz). Extensive testbed evaluations in various real-world settings and trace-driven large-scale simulations with 1100 concurrent tags were performed.

2 BACKGROUND

This section provides the technical background involved in our design.

2.1 Preliminaries

Backscatter. Advances in backscatter demonstrated ultra-low power communication at only tens of μW. The low power consumption can be achieved by reflecting the wireless signal without generating the power-hungry passband signal itself [29]. Backscatter performs amplitude, frequency, and phase modulations [36] by switching between different impedance to control the reflection coefficient [43]. The backscattered waveform is the time-domain multiplication of the excitation and the tag signals. OmniScatter tag performs FSK by switching between two impedance states, where the frequency is controlled by the switching speed.

Van Atta Array. For retro-reflectivity, Van Atta array passively reflects the signal back to the direction from which it was received without the costly beamforming circuitry. As demonstrated in Figure 1, it is a simple antenna array structure where antenna pairs are connected by symmetrical transmission lines. The transmission lines interconnect antenna elements in a way that the incident signal's phase sequence is inverted at the reflected signal to achieve retro-reflectivity. As an illustrative example, consider a four-element Van Atta array as depicted in Figure 1. An incident

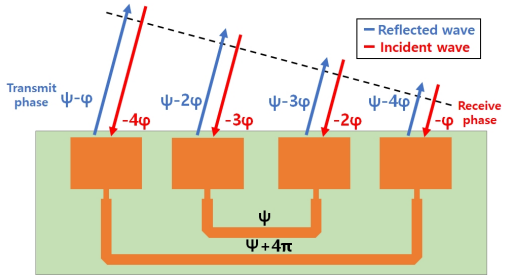

Figure 1: Van Atta array achieves retro-reflectivity through interconnection that induces phase inversion between incident and reflected signals.

signal with phase sequence of $[-4\varphi, -3\varphi, -2\varphi, -\varphi]$ produce a reflected signal with phase sequence of $[\psi-\varphi, \psi-2\varphi, \psi-3\varphi, \psi-4\varphi]$, where the phase shift from the transmission line, ψ, does not induce additional deviation of the phase interval. Therefore, the resulting phase inversion at each antenna element collectively produces the retro-reflectivity of the Van Atta array. We leverage the Van Atta array to eliminate the high beamforming overhead, as well as to mitigate multipath reflections at `OmniScatter` tag.

FMCW Radar. The FMCW (Frequency Modulated Continuous Wave) radar leverages a chirp, whose frequency linearly increases over time. A transmitted chirp bounces off surrounding objects and returns to the radar with propagation delay. Mixing the transmitted and received (i.e., delayed) chirps results in a single-tone IF signal, whose power is concentrated on a frequency proportional to the delay between the two chirps. Finally, FFT is performed on the IF signal to reveal the distance of the radar's surrounding objects. As a result, FMCW radar yields a unique distance-frequency relationship where its IF signal frequency is directly proportional to the object distance.

FMCW for mmWave Backscatter. Using FMCW as an interrogation signal for mmWave backscatter achieves significant gain, as the abundant mmWave bandwidth enables highly efficient chirp compression [1]. However, utilizing FMCW with mmWave backscatter induces high self-interference, due to the low reflection loss (i.e., stronger reflections) of mmWave signals [70]. The problem becomes increasingly significant under cluttered environments (e.g., indoors), where strong reflectors can easily overwhelm the backscattered signal. For instance, experiments showed -158.55 dB SNR in a server room while using FMCW for mmWave backscatter.

2.2 `OmniScatter` Overview

`OmniScatter` aims at a practical mmWave backscatter system by offering extreme sensitivity to enable omni-directional communication under significant attenuation (e.g., NLOS, multipath). The key enabler of `OmniScatter` is the HD-FMCW – a modified FMCW designed to support practical and robust mmWave backscatter. The `OmniScatter` consists of two main parts built on top of the unique features of HD-FMCW. The first part, discussed in Section 3, is the extreme-sensitivity mmWave backscattering. The immense sensitivity stems from HD-FMCW's powerful functionality where it leverages multiple chirp symbols to effectively isolate the ambient reflections from the tags' FSK signal in the frequency domain. This boosts SNR by over 50 dB to bring mmWave backscatter to a practical degree under harsh indoor environments combining ambient reflectors, NLOS, and blockage. The breakthrough in the SNR gain establishes reliable communication under omni-directional radar to support mobility.

Section 4 presents the second part of `OmniScatter` design – coordination-free FDMA. The coordination-free FDMA offers large-scale concurrency and excellent deployment economy by effortlessly exploiting the wide mmWave bandwidth using the radar property. Specifically, the FMCW distance-frequency relation automatically assigns separate channels to tags according to the tag-radar distance. In addition, HD-FMCW can be configured for optimal scalability. In essence, HD-FMCW's chirp duration parameter controls dissecting the entire mmWave bandwidth into channels and allocating them to the tags. The number of chirps per symbol controls multiplexing within the same channel by controlling the number of tag bins. Carefully setting chirp and symbol duration collectively achieves optimal spectrum utilization to reach maximum scalability.

3 EXTREME SENSITIVITY COMMUNICATION

In this section, we discuss the technical details of `OmniScatter`, including the core mechanism of HD-FMCW that enables robust communication.

3.1 High Definition FMCW

FMCW, by leveraging the chirp spanning the entire bandwidth, offers a substantial amount of coding gain to potentially aid the low power backscatter signal otherwise undetectable. However, typical indoor spaces like homes, offices, malls and hospitals have a complex environment with rich ambient reflections, where they quickly add up to an extensive amount of clutter noise. This essentially causes a strong self-interference that easily dominates over the weak backscatter signal.

`OmniScatter` presents HD-FMCW, which effectively addresses the clutter noise problem while keeping the benefit of the FMCW intact. HD-FMCW disentangles the overwhelming clutter noise (i.e., ambient reflections) from the tag signal in the frequency domain. This boosts tag signal SNR by over 50 dB improvement over the original FMCW. HD-FMCW thus enables reaching `OmniScatter` tags deployed in a practical, non-line of sight settings – including the ones that are stored in cabinets and packaged in boxes. In the meantime, HD-FMCW remains economic where it is compatible with commodity low-cost radars and does not incur extra computation over the original FMCW.

HD-FMCW (like the original FMCW) leverages chirps, is monostatic, and computes the IF signal by multiplying the transmitted and the reflected chirps, on which FFT is performed to obtain the location represented as an FFT bin. Such similarity lets HD-FMCW be implemented on commodity FMCW radars, ensuring affordability (section 5.2). On the other hand, HD-FMCW departs from the original FMCW mainly in two aspects: (i) HD-FMCW holds a series of chirps per symbol without inter-chirp gaps, as opposed to a single-chirp symbol with guard time in FMCW. (ii) The phase is kept continuous throughout the chirps within the symbol. That is,

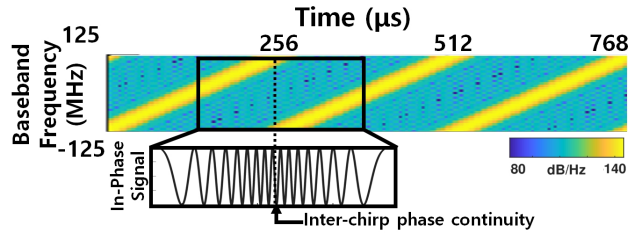

Figure 2: An HD-FMCW symbol with 3 chirps and continuous inter-chirp phase.

the phases at the beginning and the end of a chirp are matched in HD-FMCW for periodicity among chirps. Figure 2 demonstrates HD-FMCW with 3 chirps, 256μs chirp duration, and 250 MHz bandwidth in the 24 GHz band. The multi-chirp symbol design in HD-FMCW enlarges the number of samples per symbol, which indicates a higher number of FFT bins, or equivalently, enhanced frequency resolution (= bandwidth/sample). For instance, Figure 2 yields the frequency resolution of $1302Hz$ ($=\frac{1}{3\times256\mu s}$).

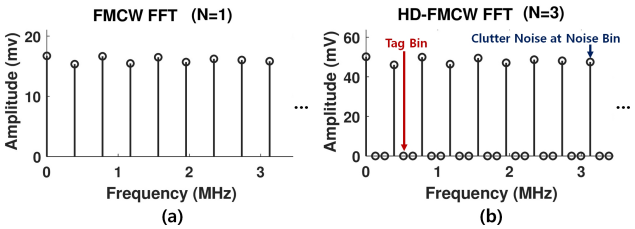

Figure 3: (a) The FFT result of FMCW, and (b) the FFT result of HD-FMCW with $N = 3$ chirp symbol. $N - 1 = 2$ tag bins are placed in between the noise bins.

By the FFT property, FFT of an N repetition signal corresponds to the FFT of a single instance where each bin is followed by $N - 1$ extra bins, whose values are zeros [2]. Likewise, in N-chirp HD-FMCW, the periodicity of the chirps yields FFT of a single chirp with $N-1$ zero bins between each non-zero bin. That is, compared to the original FMCW, multi-chirp HD-FMCW increases the frequency resolution to introduce extra FFT bins, where they all hold zeros. In other words, reflected signals (i.e., clutter noise) are strictly limited to non-zero bins repeated every N bins (hereafter *noise bins*).

Figure 3(a) illustrates the FFT of FMCW ($N = 1$), while figure 3(b) illustrates the HD-FMCW ($N = 3$) to show the clutter noise captured in noise bins repeated every $N = 3$ bins. Other bins (holding zeros) are exclusively allocated to FSK-modulated tag signals (hereafter *tag bins*). That is, unlike clutter noise, FSK is able to slide the signal into the tag bins[1]. Tag bins in Figure 3 are empty as no tag signals are present. Isolating noise bins from tag bins essentially achieves frequency-division multiplexing between the noise and the tag signal. The tag's signals are safeguarded in the tag bins, intrinsically unaffected by the environment. This enables extreme sensitivity and robust communication regardless of the surroundings and scenarios, including NLOS and blockage. In the following, we provide the rigorous derivation of HD-FMCW.

[1]In principle, this is due to the inter-chirp phase discontinuity induced by the FSK modulation.

HD-FMCW Derivation. The reason behind the periodic noise bins (and tag bins in between) is the unique design of HD-FMCW leveraging the periodic chirp symbol; If we let T seconds denote the chirp duration, an HD-FMCW symbol is a periodic signal with T which is represented as a signal at multiples of $1/T$ Hz (i.e., periodic FFT bins in multiples of $1/T$ Hz) in the frequency domain. A strict derivation for this is as follows. Let $c(t)$ denote a chirp with duration T. Then the multi-chirp symbol $s(t)$ with N chirps is denoted as

$$s(t) = c(t) * \sum_{n=1}^{N} \delta(t - nT) \tag{1}$$

where $\sum \delta(t - nT)$ is a impulse train with interval T. After $s(t)$ is emitted from the HD-FMCW radar, it bounces off an object and returns to the radar with attenuated and time delayed chirps. That is, the reflected signal $s'(t) = \alpha c(t - \Delta t) * \sum_{n=1}^{N} \delta(t - nT)$ where α and Δt are the attenuation and time delay, respectively. HD-FMCW runs FFT on the product of emitted and reflected signals – that is,

$$\mathbf{F}\Big\{s(t)s'(t)\Big\} = \alpha\mathbf{F}\Big\{c(t)c(t-\Delta t)\Big\} \cdot \sum_{n=-\infty}^{\infty} \delta\left(f - n\frac{1}{T}\right) \tag{2}$$

which yields impulse train with interval $1/T$ weighted by $\alpha\mathbf{F}\{c(t)c(t-\Delta t)\}$. The FFT bins at which the impulses are located are the noise bins. All clutter noise is concentrated on the corresponding bins where the tag bins only hold FSK-modulated tag signal. Figure 3 is a case of a 3-chirp symbol ($N = 3$) with the noise bin in the multiples of $1/T$ Hz. The frequency resolution of $\frac{1}{NT}$ Hz produces N FFT bins every $1/T$ Hz, which consists of 1 noise bin and $N - 1$ tag bins.

Note that, for the sake of understanding, Eq. 2 is derived under a simplified scenario with a single reflection. In practice, multiple reflections occur by various objects and surroundings, where the same principle of noise and tag bins holds. Specifically, Eq. 2 is extended to

$$\sum_{l=1}^{L} \alpha_l \mathbf{F}\Big\{c(t)c(t-\Delta t_l)\Big\} \cdot \sum_{n=-\infty}^{\infty} \delta\left(f - n\frac{1}{T}\right) \tag{3}$$

where L is the number of reflections. This indicates that, even in the face of multiple reflections, the clutter noise is effectively accumulated on the noise bins without occupying the tag bins. That is, the efficacy of the clutter noise rejection in HD-FMCW generally holds in practical settings. The tags bins are exclusively reserved for the FSK-modulated tag signals. The following section provides details on how FSK-modulated tag signals are allocated in the tag bins as well as how they are demodulated.

HD-FMCW on Commodity mmWave Radar. `OmniScatter` is compatible with various commodity mmWave radars which yield physical layer samples for signal analysis [13, 23, 58]. Briefly, this is achieved by compensating the inter-chirp phase gaps, such that the phase remains continuous throughout the chirps in a `OmniScatter` symbol. We discuss the details in the implementation section 5 and provide extensive evaluation on two popular commodity mmWave radars of EVAL-Tinyrad [13] and mmWaveICBoost [23]. To ensure general applicability, we choose the radars from different vendors (Analog Devices and TI) spanning disparate mmWave bands of 24 GHz and 60 GHz.

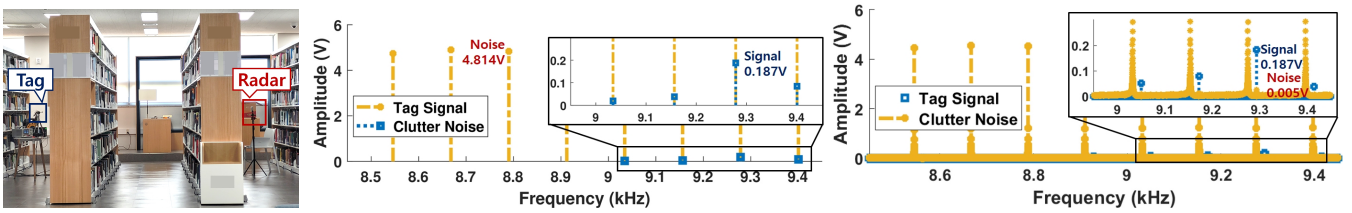

(a) NLOS in library (b) FMCW FFT (c) HD-FMCW FFT

Figure 4: The SNR gain and tag signal demodulation of (HD-)FMCW.

3.2 Lightweight (De)modulation

OmniScatter offers lightweight and highly robust (de)-modulation. At the modulation side, the tag overhead is minimized by adopting FSK that can be effectively implemented under a simple architecture – impedance switching at the speed of modulation frequency, f_m. FSK by f_m yields time-domain multiplication of $e^{j2\pi f_m t}$ to the reflected signal [29]. In other words, the HD-FMCW FFT result for tag signal can be computed by substituting $s'(t)$ in Eq. 2 with $s'(t)e^{j(2\pi f_m t)}$ which yields $\mathbf{F}\{s(t)s'(t)\} * \delta(f - f_m)$. Therefore, the HD-FMCW FFT result of the tag, compared to the ambient reflectors, is fine-tuned in frequency to shift into a tag bin that is f_m away from the noise bin. Specifically, the tag signal is represented as multiple peaks due to spectral leakage in DFT [19] where peaks all show the same frequency shift of f_m. Again, by DFT, the amplitudes follow the sinc function, where up to four peaks (centering the main lobe) are apparent where others are negligible (e.g., > 13 dB lower than the main lobe).

Given the tag signal peaks, the demodulation is simply capturing the highest peak within four adjacent peaks with the same frequency offset. By doing so we avoid misunderstanding the multiple peaks as different tag signals when multiple tags are deployed, and also keep the demodulation process consistent under multiple tags. This demonstrates extremely lightweight OmniScatter demodulation with a negligible overhead on top of default FFT operation of commodity FMCW radar. The uncontaminated tag signal offers > 50 dB boosted SNR for highly robust demodulation. Figure 4 demonstrates the SNR gain of HD-FMCW in comparison to FMCW in an NLOS scenario. Figure 4(b) demonstrates FMCW SNR of -28.21 dB (=$20\log_{10}\frac{0.187}{4.814}$), where-as figure 4(c) demonstrates HD-FMCW SNR to 31.46 dB (=$20\log_{10}\frac{0.187}{0.005}$), indicating SNR gain of 59.67 dB. Extensive evaluation under the NLOS communication settings showed an average SNR gain of 51.84 dB out of total 1024 symbols measured, where minimum signal strength for communication (i.e., OmniScatter sensitivity) was at -115 dBm. We can observe that the zero bins in figure 4(c) have near-zero noise, which stems from various noise sources including thermal noise. Furthermore, OmniScatter simultaneously demodulates multiple tag signals in a single FFT operation, offering unique benefits for OmniScatter at scale.

4 COORDINATION-FREE FDMA

This section discusses how OmniScatter effectively utilizes the wide mmWave bandwidth in a coordination-free fashion for deployment economy and scalability, through the combination of the distance-frequency relationship and the chirp configuration in HD-FMCW.

4.1 Distance-based Automatic Ch. Allocation

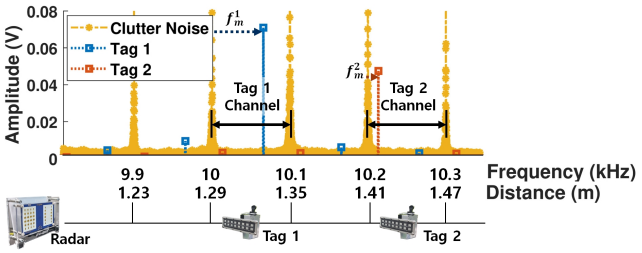

Figure 5: Signal demodulation of multiple (two) tags at 1.32m and 1.44m distance. Tag 1 and Tag 2 are modulating frequency at f_m^1 and f_m^2.

HD-FMCW's extreme sensitivity in combination with the wide bandwidth of mmWave, spanning as large as 14 GHz (60 GHz band), offers an ample opportunity to support tags at scale. However, this requires addressing several technical challenges to reach practicality. This includes minimizing the control overhead and (de)modulation complexity to avoid prohibitively high coordination and communication costs under a large body of devices. Strictly-constrained backscatter systems impose further challenges; In particular, due to the extremely limited power budget, backscatters are equipped with a low-end LO (or even lack LO), typically ranging at most tens of MHz [72]. This indicates that backscatter FSK cannot modulate through the mmWave spectrum ranging from hundreds to thousands of MHz – thus limiting backscatter from leveraging the wide mmWave bandwidth. Furthermore, the absence of costly bandpass filters in backscatters incurs difficulty in multiplexing and vulnerability to inter-tag interference, whose impact would significantly grow with scale.

Without relying on LO and passband filter for channel switching, as demonstrated in Figure 5, OmniScatter is uniquely designed to exploit the radar property so as to passively and automatically assign separate channels to tags according to the tag-radar distances. Essentially achieving coordination-free FDMA spanning the entire mmWave bandwidth without incurring any overhead to both tags and radar. The channels are separated by the noise bins, indicating the channel width of $1/T$ Hz and the inter-channel distance (i.e., the minimum spacing between tags to be allocated at different channels) of $\frac{c}{2BW}$m [48]. Tags are passively allocated with the corresponding channels by their tag-radar distances. Tags simply modulate FSK within the channel width of $1/T$ Hz for channel access, without any knowledge on which channel they are assigned to.

Another advantage of coordination-free FDMA is that the tag operation is kept identical to the single tag scenario – i.e., tags greedily modulate without considering other tags. Lightweight demodulation is also retained where the HD-FMCW radar simultaneously demodulates all tags with a *single* FFT operation followed by a linear search along the frequency in the FFT output. Such features make `OmniScatter` a highly efficient solution for various practical settings.

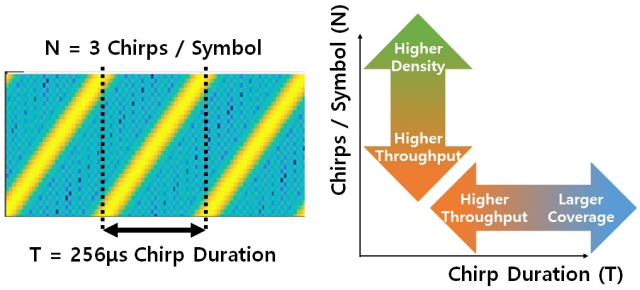

Figure 6: The coverage of HD-FMCW grows proportional to chirp duration T and the density grows proportional to the number of chirps $N-1$. The chirp duration and samples per chirp collectively form the per-tag throughput proportional to $\frac{1}{T \times N}$.

4.2 HD-FMCW Configuration

The number of channels given in the distance-based channel allocation is highly variant depending on the bandwidth. For instance, 60 GHz band with 14 GHz bandwidth reaches up to 4600 channels for deployment diameter D=50m, whereas it is limited to just over 80 for 24 GHz band with 250 MHz bandwidth, for the same D. Similarly, inter-channel distance varies widely; 10.7 mm and 600 mm for 60 GHz and 24 GHz, respectively. In other words, the number of channels and the inter-channel distance are decided by the bandwidth and thus is uncontrollable, and granting a channel to a single tag may not provide sufficient room for a dense deployment scenario. As depicted in Figure 6, `OmniScatter` support disparate performance demands and deployment settings simply by configuring the chirp duration (T) and the number of chirps per symbol (N).

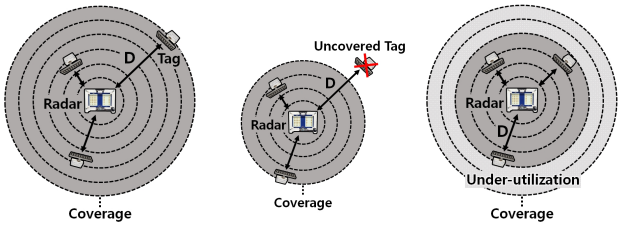

(a) Optimal (b) Uncovered (c) Under-utilized

Figure 7: Various spectrum utilization scenarios with different chirp duration, T.

Chirp Duration (T). `OmniScatter` optimizes the utilization of the mmWave bandwidth by aligning the radar coverage with the deployment diameter, D, which is the maximum tag-radar distance in the deployment. Optimizing the channel utilization enables `OmniScatter` to (i) exploit the entire mmWave bandwidth and (ii) maximize the tag bins in a channel to reach the maximum scalability, while (iii) the entire nodes are covered. This is achieved by maximizing the channel width, $1/T$ Hz; Or equivalently, minimizing the chirp duration T (=maximizing chirp slope), under the condition that the transmitted chirp overlaps with the received chirp, which is the basic requirement for (HD-FMCW) radar. This yields the minimum T of $2D/c$. Figure 7 (a) demonstrates the optimal configuration with the maximum channel width while all nodes fall within the radar range. On the contrary, Figure 7 (b), (c) depicts mismatch between D and the radar coverage. Figure 7 (b) demonstrates uncovered tag and Figure 7 (c) depicts spectrum under-utilization (i.e., not all bandwidth is used) which are both undesired. Minimized chirp duration, or maximized channel width in Figure 7 (a) indicates more chirps while the symbol duration is kept the same – In other words, more tag bins for the same amount of time to improve scalability and bitrate.

# of Chirps per Symbol (N). Multiplexing among multiple nearby tags within the same channel begins by increasing the number of tag bins. This is easily configured by the number of chirps per symbol, N. Given the rich tag bins within a channel, each tag is granted an independent subset of bins within a channel for multiplexing. Note that this can be achieved coordination-free, simply by letting tags access a set of bins whose bits incorporate the corresponding tag id. For this, the number of chirps per symbol is configured such that bits per symbol is larger than the tag id space. Specifically, N chirps per symbol (=$\log(N-1)$ bits per symbol) scales to $\frac{N-1}{2}$ tags under 2-FSK. We note that increasing the tag bins comes at the cost of lower throughput (i.e., $\frac{log_2((N-1)/k)}{N \cdot T}$, where k is the number of tags sharing a channel) due to increased symbol duration. That is, a 2-FSK tag's throughput reduces by N/N' when chirps increase $N \rightarrow N'$. Our evaluation configuration of 2048 chirps per symbol and chirp duration T = 40.96 μs, in combination with tags utilizing a typical crystal oscillator of 150ppm accuracy, supports 1023 unique ids where each tag concurrently transmits at 12 bits per second.

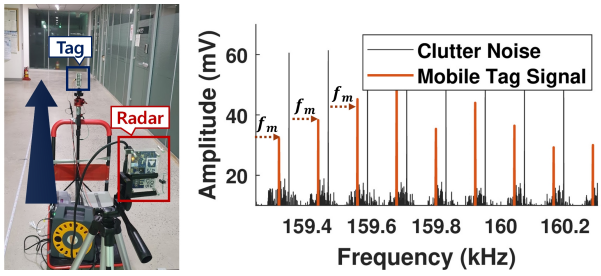

Figure 8: The spectral leakage in a mobile tag.

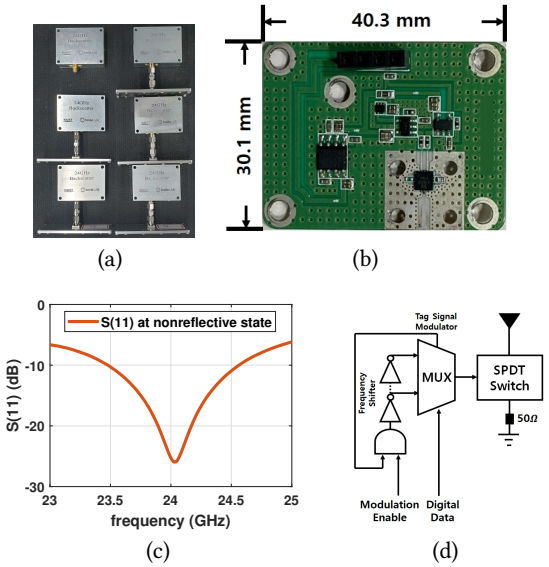

Figure 9: (a) 6 of our mmWave tags inside the aluminum casing. (b) Our mmWave tag board. (c) The S(11) parameter of our tag at 50 Ω matched ground (non-reflective) state. (d) The tag's circuit diagram.

4.3 Mobility Support

Beamforming and alignment are widely used in mmWave to compensate for the substantial signal attenuation at the cost of imposing a significant bottleneck for mobility. Unlike this common practice, `OmniScatter`, with over 50 dB SNR gain, achieves reliable communication under omni-directional radar (i.e., without beamforming and alignment) and retro-reflective (e.g., Van Atta array) tags. This lays a solid foundation for the mobility support in `OmniScatter`. In fact, `OmniScatter` inherently offers seamless connectivity for mobile tags without any additional design – i.e., identical modulation applies for stationary and mobile tags. A minimal change at the radar side radar suffices, where it enlarges the demodulation window from four (section3.2) to a larger value according to the tag movement speed. This is because a mobile tag may traverse multiple channels within the symbol duration, which expands the spectral leakage to several channels beyond four for stationary tags. Figure 8 depicts the experimental tag signal measured at walking speed (≈ 1.4 m/s) with the 262 ms symbol duration, demonstrating spectral leakage across 9 channels. To reflect this, the demodulation window is set accordingly.

5 IMPLEMENTATION

This section presents the implementation details of `OmniScatter`. We implement HD-FMCW on three different commodity mmWave radars, as well as our own custom reader backend. Three different versions of mmWave backscatter tags are developed to operate as `OmniScatter` tag.

5.1 `OmniScatter` Tag Prototype

Figure 9(a)-(b) show the prototype of 24 GHz `OmniScatter` tag implemented on Rogers RO4003C substrate with MACOM MASW-011105 GaAs SPDT RF switch. The RFC port of the switch is connected to the commodity 24 GHz 17 dBi microstrip array antenna,

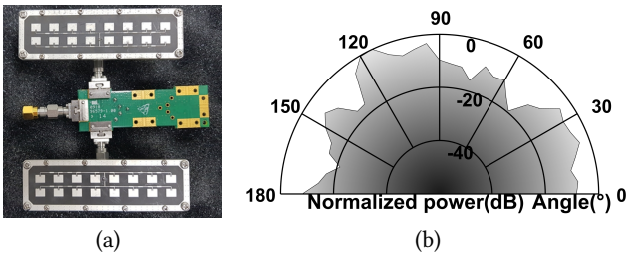

Figure 10: (a) Prototype tag with Van Atta array antenna, and (b) beam pattern (retro-reflectivity)

and the RF1 / RF2 ports are connected to 50 Ω matched ground (non-reflective) and open (reflective). The tag performs FSK by switching between RF1 and RF2 ports, essentially controlling the reflectivity over time. Figure 9 (c) depicts the measurement result of the return loss (S(11)) at 50 Ω matched ground. The return loss is flat -9.5 dB at the reflective state, leading to a difference of over 20 dB between the switch states. For tag control signal, either Altera TerasIC T-Core P0633 FPGA board or Arduino Uno were used. The form factor is 40.3 × 30.1mm.

Power Consumption. The tag uses MACOM RF switch with $5\mu W$ power consumption. For power consumption analysis, we design a 2-FSK backscatter tag and simulate an IC for the control board using Libero SoC SmartPower [6], as shown in Figure 9(d). A ring oscillator and modulator circuit with a power consumption of $2\mu W$ are used for frequency shift and control logic. The total power consumption is $7\mu W$ (well below the 33 μW energy harvesting [72]), which can operate battery-free, or with a coin cell battery of 1000 mAh for 48.9 years.

Implementation Cost. The tag can be produced at a reasonable price of 25.528 USD. This consists of Macom MASW-011105 switch (20 USD), Rogers RO4003C substrate (0.028 USD considering the required substrate size), and an Arduino Uno (5 USD) with a signal inverter (0.5 USD) for control. Figure 10 presents our Van Atta prototype tag, built on EVAL-ADRF5026 board and commodity 24 GHz antennas. Figure 10 depicts beam pattern measurement of the Van Atta tag showing the retro-reflective operation of over -20 dB over the full 180 degrees of incident angle. The retro-reflectivity of Van Atta tag alleviates the high beamforming overhead, and suppresses the multipath effect at `OmniScatter`. Our 60 GHz tag uses V-Band Reflective SPST PIN Diode Switch (Eravant), with WR-15 Waveguide Horn Antenna (Pasternack) and WR-15 WAVEGUIDE OPEN (Eravant).

5.2 `OmniScatter` Reader Implementation

Reader implementation on 24 GHz commodity radars was made on Distance2Go (Infineon) and EVAL-Tinyrad (Analog Devices), while mmWaveICBoost, IWR6843ISK antenna, and DCA1000EVM interface boards were used for 60 GHz radar. The commodity radars in our testbeds range from 200 [58] to 1500 USD [13] (Note that 900 MHz RFID readers typically range between 1000 and 2000 USD [5]). Implementation of `OmniScatter` on commodity radars only requires signal processing without any changes to the physical layer.

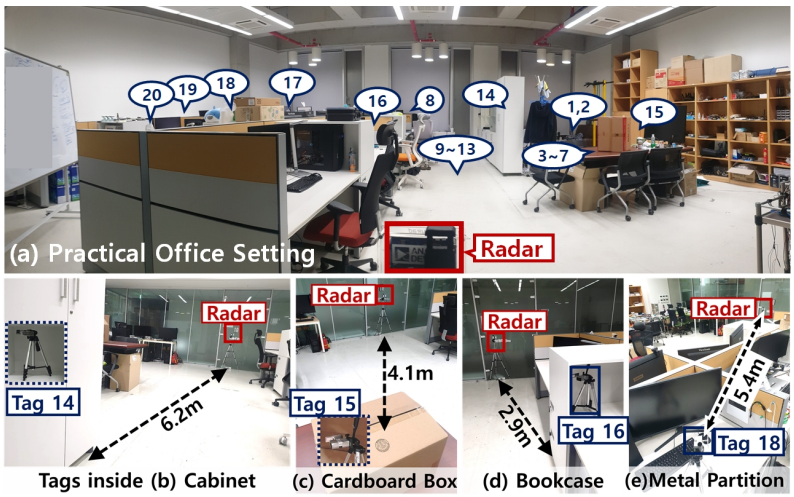

Figure 11: `OmniScatter` evaluation in a practical office setting of approx 10 x 10m. Radar is omni-directional. Some tags are enclosed in a wooden cabinet (tag 14), packaged in a cardboard box (tag 15), hidden behind a wooden bookcase (tag 16), and obstructed by metal partitions (tag 18).

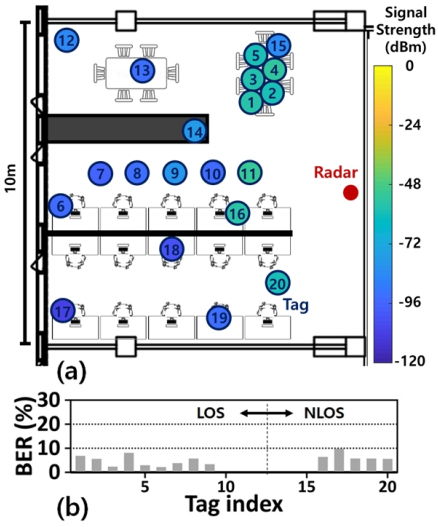

Figure 12: (a) Signal strength and (b) BER of the tag with a single omni-directional radar. Signal strength as low as -103.6 dBm achieves < 10% BER

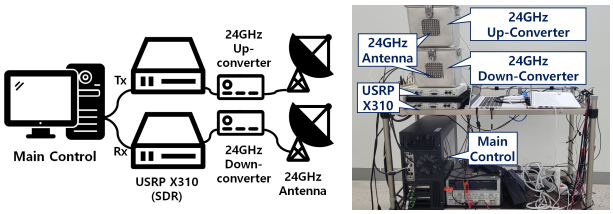

Figure 13: `OmniScatter` custom reader backend (a) schematic diagram and (b) snapshot.

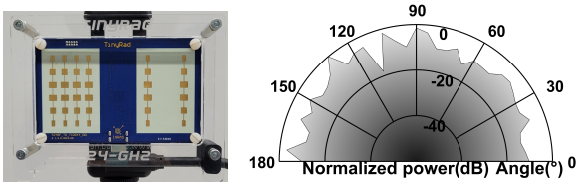

Figure 14: (a) `OmniScatter` reader implemented on Eval-Tinyrad, and (b) the single Tx antenna omni-directional beam pattern

This is enabled by reconstructing the received signal to compensate for the phase offset, so as to emulate the phase continuous HD-FMCW. The chirp signals are carefully concatenated to keep the phase continuity of the tag signal, where the inter-chirp interval is known and set using the customized chirp parameters. An SDR-based testbed is implemented for in-depth analysis. The 24 GHz testbed in Figure 13 uses two USRP X310s for Tx and Rx, operating through up and down converters (EVAL-ADMV1013, EVAL-ADMV1014) quadrupled from 6 GHz external LO.

6 EVALUATION

In this section, we perform extensive experiments to evaluate `OmniScatter` performance under various circumstances. Specifically, we demonstrate (i) the practicality of `OmniScatter` system by deploying our tags in blockage and multipath rich environments with discrete communication distances, (ii) the massiveness of `OmniScatter` by simulating concurrent communication with trace-based experiments, (iii) the SNR gain of `OmniScatter` by comparing the SNR of HD-FMCW with basic FMCW system, and (iv) the mobile communication performance of `OmniScatter`.

We evaluate `OmniScatter` performance using the EVAL-Tinyrad commodity radar as a reader, combined with our 24 GHz prototype tag. The radar is set to use a single Tx and single Rx antenna to simulate omni-directional reader. The radar snapshot and experiment results of the antenna beam pattern are shown in Figure 14. The radar is configured to have maximum transmission power of 8 dBm, and utilizes the full 250 MHz bandwidth of the 24 GHz ISM band (24-24.25 GHz). For each evaluation 128 symbols are transmitted and received, where each symbol consisted of 32 chirps with 8.192 *ms* chirp duration and 23 μs inter-chirp guard-time.

6.1 Practical Deployment and Communication

Figure 11 and 12 demonstrate the practical deployment and communication of `OmniScatter`. The tags were deployed in various locations throughout the office space of $10m \times 10m$, consisting of various LOS and NLOS communication paths. Among all tag locations in Figure 11(a), at most 4 locations were repeatedly chosen and evaluated with each tag modulating at different frequencies of 150, 152, 154, and 156 kHz. The tags simultaneously transmit data, where the signal strength and BER are measured to plot the signal strength heatmap and BER graph in Figure 12. The radar's orientation and location were fixed throughout the experiment, to show the beamforming-free operation of `OmniScatter`. The result

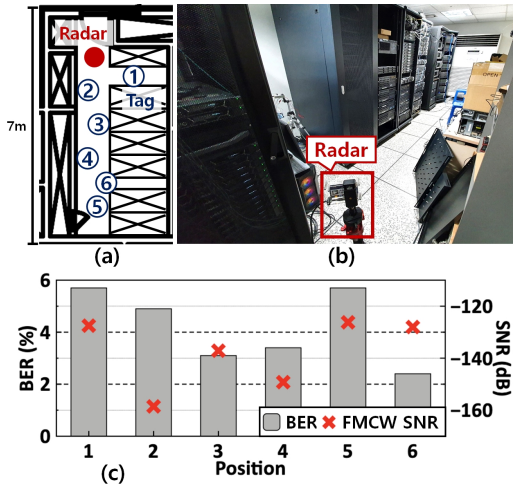

Figure 15: Cluttered environment communication evaluation. (a) The tag deployment, and (b) the on-site view, and the (c) BER and SNR of the evaluation is depicted.

shows that with signal strength as low as -103 dBm, OmniScatter achieves BER of under 10%. Hence, the reception probability of OmniScatter can effectively reach under 1% with 2 repeated transmissions [35], proving the practicality of our design. We note that the control signal for the 24 GHz prototype tag was provided by Arduino Uno [3], where the high thermal sensitivity of its oscillator (>3% error in operating temperature [4]) contributed to the relatively high BER of up to 10% in OmniScatter evaluation. The BER can be significantly reduced by implementing a simple error-correcting code (e.g., forward error correction), or by implementing a temperature-robust control board hardware (e.g., temperature compensated crystal oscillators).

6.2 Cluttered Environment

Figure 15 demonstrates OmniScatter's ability to communicate at highly cluttered environment, by demonstrating the performance under rich multipath and blockage. The experiment was conducted in a server room, where multiple metal racks were cluttered. Total 6 locations in Figure 15(a),(b) are tested with the tag, with modulation frequency of 156 kHz. The SNR and BER measured from 6 tag locations are shown in Figure 15(c), where BER is kept under 6% with a significantly low FMCW SNR (i.e., without HD-FMCW implementation) of -158 dB. The successful communication under the harsh cluttered environment is made possible by the powerful SNR gain and clutter noise rejection of HD-FMCW design. The evaluation verifies the robustness of OmniScatter under complicated and realistic cluttered environment scenarios.

Blockage Penetration. Table 2 demonstrates our design's performance under common indoor blockages; paper box, glass window, plaster wall, and wooden door, each with a thickness of 5mm, 10mm, 130mm, and 40mm. The tag was completely surrounded by the blockage material, such that there was only a penetration path to communicate with the radar. The tag modulates at 156 kHz for the experiment. Each experiment was conducted on 1.2m distance space between tag and radar. The table compares the SNR of

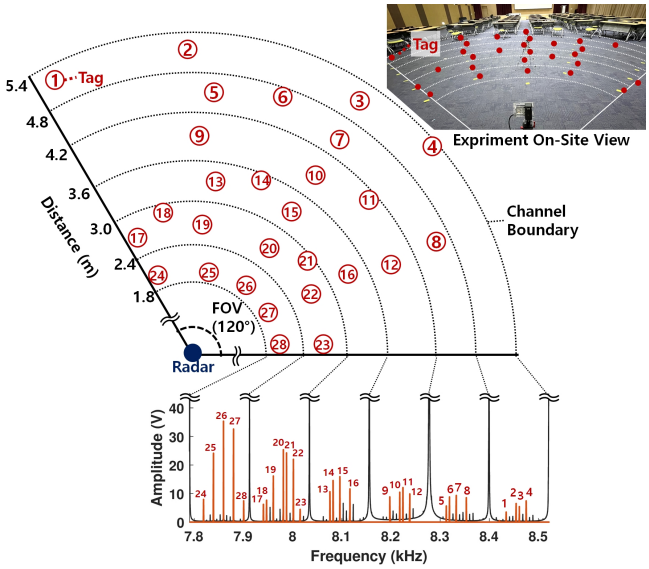

Figure 16: The tag deployment of distance-based channel allocation evaluation, and the representation of corresponding tags at HD-FMCW FFT.

Blockage Materials	FMCW SNR (dB)	HD-FMCW SNR (dB)	OmniScatter BER (%)
No Blockage	15.46	51.92	1.60
Box	-2.77	48.87	3.36
Glass	5.33	48.95	1.60
Plaster	-15.65	45.93	6.73
Wood	-35.31	39.53	3.36

Table 2: Different penetration materials and the corresponding SNR, BER results.

OmniScatter with FMCW under different blockages. The highly efficient clutter noise rejection and SNR gain of HD-FMCW show prominent SNR and BER even under blockage scenario, with a high SNR gain of over 50 dB and maximum BER of 6.7%. The results verify the communication stability under various blockages and demonstrate the possibility of communicating with tags at isolated locations.

6.3 Distance-based Channel Allocation

In order to verify the distance-based channel allocation ability of OmniScatter, a trace-based experiment consisting of 28 different location-frequency pairs was conducted. The tag-reader distance ranged from 1.8m to 5.4m, and each tag modulated at frequencies of 7315 Hz to 7411 Hz. The evaluation was conducted by recording the tag signal at all 28 different location-frequency pairs, then summing all the signals to run FFT on the summed data. The tag deployment and the representation of each corresponding tag at HD-FMCW FFT are depicted in the Figure 16. The FFT results show successful distance-based channel allocation at of OmniScatter, where tags at different distances are allocated to their corresponding channel.

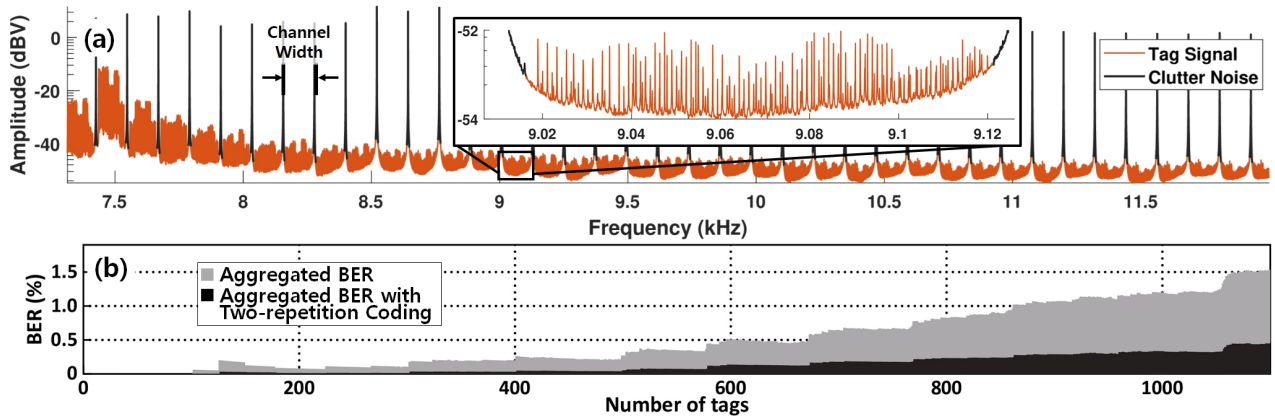

Figure 17: Trace-driven large-scale evaluation. (a) demonstrates the 1100 tag signals across channels. (b) depicts the BER of the entire tags. HD-FMCW effectively rejects noise to keep BER at a practical level of below 1.5%

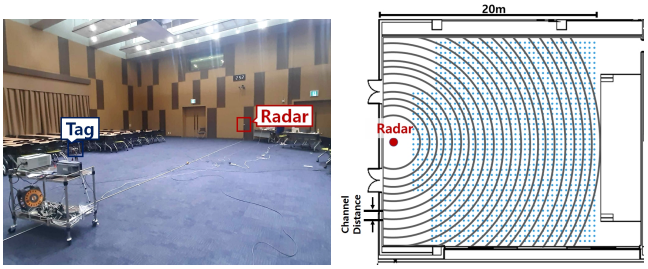

(a) (b)

Figure 18: Large-scale evaluation in a auditorium of over 20m × 20m: (a) on-site view and (b) deployment scenario where the blue dots and coaxial circles indicate tags and channels, respectively.

6.4 Large-scale Trace-driven Evaluation

To verify the massive operation of `OmniScatter`, a large-scale trace-driven experiment consisting of 1100 different location-frequency pairs in an auditorium of $20m \times 20m$ size was conducted, as shown in Figure 18. The tag-reader distance ranged from 0.3m to 14.1m, while the modulation frequency ranged from 7315 Hz to 7414 Hz, occupying a total of 4 kHz bandwidth out of 250 MHz at the radar side. The trace-driven experiment was conducted by recording the tag signal at all 1100 different location-frequency pairs, then summing all the signals to verify if 1100 tag concurrent communication is possible at `OmniScatter` design. Figure 17(a) shows a partially enlarged HD-FMCW FFT result of the summed signal, where it can be clearly seen that the distance-based FDMA of our system has located each tag at different channels. The multiple channel access of `OmniScatter` is also demonstrated, where over 45 tags share the channel without collision. Figure 17(b) shows aggregated BER after the summation of signals, plotted with respect to the number of aggregated tags. The tag signals are summed in the order of increasing communication distance. The demodulation of 1100 added tag signals stay under 2% BER, which results in <0.35% BER after forward error correction (FEC) of two repetitions is applied. The BER results show the capability of `OmniScatter` massive operation. We observe that the aggregated BER increases with the increase of the number of added tags, since the tags added later will have larger noise due to the longer communication distance. Also, as the signal is summed up, the AWGN noise is also added altogether, leading to conditions that may be harsher than practical scenarios. Still, `OmniScatter` is able to demodulate each and every signal successfully. This is made possible by efficient clutter noise rejection of HD-FMCW, in combination with `OmniScatter` channel allocation design. As a result, `OmniScatter` tags can robustly operate under massive, concurrent scenarios.

6.5 HD-FMCW SNR Gain

We evaluate the SNR Gain from HD-FMCW clutter-noise rejection under multiple distances in the hallway and outdoor, as shown in Figure 19(d). A tag modulating at 150 kHz was used for the experiment. The SNR gain of our system is demonstrated by comparing the SNR of HD-FMCW system against the basic FMCW system. The SNR gain of HD-FMCW is clearly visible in Figure 19(a),(b), where the results show that our system achieves SNR gain of over 54 dB under outdoor scenarios, and SNR gain of over 60 dB under hallway scenarios. The higher SNR gain under the hallway scenario is due to the larger clutter noise in the hallway, where the HD-FMCW clutter-noise rejection plays a critical role in separating the noise from the signal. As shown in Figure 19(c), the high SNR gain of our system enables communication in long distances, where the BER remains under 10% up to 40m and 30m in the outdoor and hallway scenario, respectively. This is especially meaningful considering that the communication distances were achieved without beamforming (i.e., single Tx and Rx antenna element of radar was used). The results illustrate efficient clutter noise rejection of HD-FMCW producing high SNR gain, where it enables large area deployment of `OmniScatter`.

HD-FMCW at 60 GHz. Figure 20(a) further demonstrates our design's compatibility with 60 GHz systems. The experiment was conducted in hallway using 60 GHz radar with our 60 GHz backscatter tag, modulating at 210 kHz. At the radar side, the bandwidth of

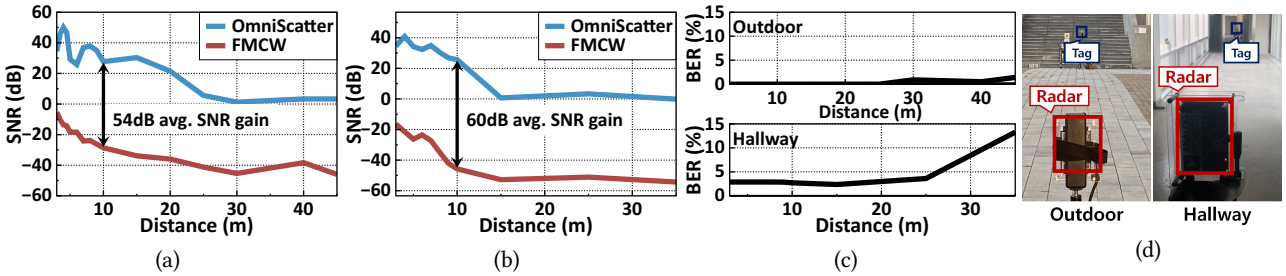

Figure 19: (a) Outdoor SNR gain according to communication distance. (b) The SNR gain at hallway according to communication distance. (c) The BER of corresponding experiments. (d) Snapshot of each experiment scenarios.

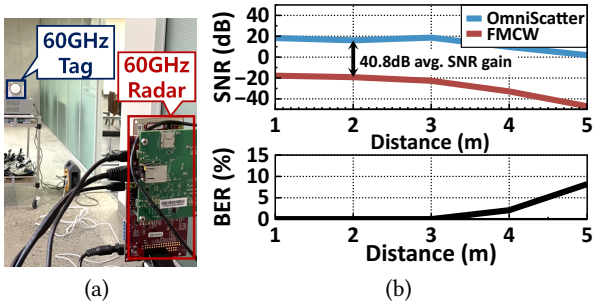

Figure 20: The SNR gain and BER according to distance for 60 GHz `OmniScatter`

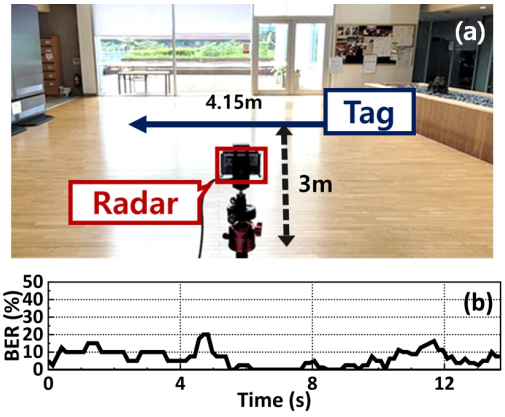

Figure 21: BER by time under horizontal tag movement. The tag is moved at uniform speed in a straight line, with a minimum 3m distance from the radar.

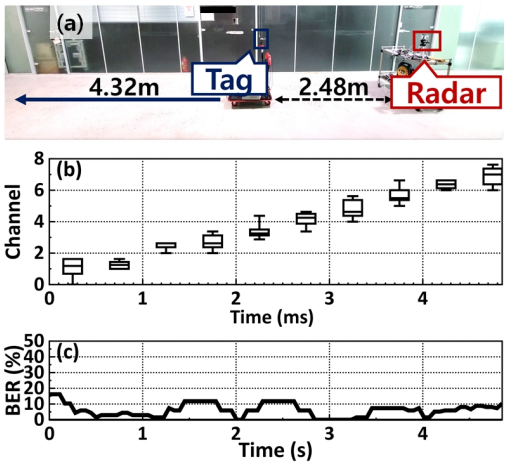

Figure 22: BER along perpendicular movement from the radar, and the resulting channel shift. The tag is moved from 2.48m to 6.8m distance to the radar.

1.8 GHz was used (60.25 GHz to 62.05 GHz), where the chirp duration, inter-chirp guard-time, and the number of chirps per symbol were each set to be 25.6μs, 134.4μs, and 128, respectively. Total of 40 symbols were transmitted and received for evaluation. The SNR gain is demonstrated by comparing the SNR with and without the HD-FMCW according to distance in Figure 20(b), followed by the corresponding BER analysis. Results show that a minimum 36 dB SNR gain was achievable at 60 GHz, with BER under 10% up to 5-meter distance. The experiment result proves the versatility of our system to frequencies higher than 60 GHz for future compatibility.

6.6 Mobile Scenario

Figure 21, 22 depict the mobile performance. As `OmniScatter` does not require beamforming at the reader side, mobile tags can be successfully detected and demodulated under mobility. For the mobile experiment, the number of chirps per symbol was set to 8, where a total of 1664 symbols were transmitted and received for evaluation. Figure 21(a) depicts the simple indoor mobility experiment conducted, where the tag is moved 4.15m horizontally in a straight line, with a minimum 3m distance from the radar. The measurement is made over the time of 13.7s, with velocity of 0.3m/s. Figure 21(b) depicts the BER over time, where the average BER of the travel is 6.4%. Figure 22(a) depicts another indoor mobility, where the tag is perpendicularly moved 4.32m (from 2.48m to 6.8m) in a straight line over the time of 48.5s, with velocity of 0.9m/s. Figure 22(c) depicts the BER over time, where the average BER of the travel is 6.2%. The tag modulates at 156 kHz for both experiments. The plot depicts successful tag communication in mobility. Figure 22(b) depicts the channel allocation according to radar-tag distance, where the channel is shifted as the communication distance increases. The results verify the mobile communication support of `OmniScatter`.

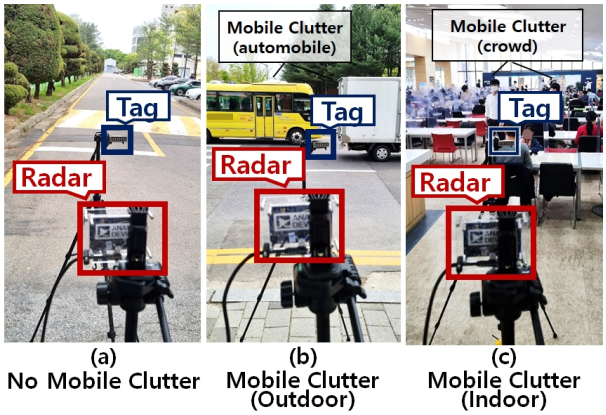

Figure 23: Snapshot of experiment scenario under (a) no mobile clutter, (b) outdoor mobile clutter (roadside), and (c) indoor mobile clutter (cafeteria).

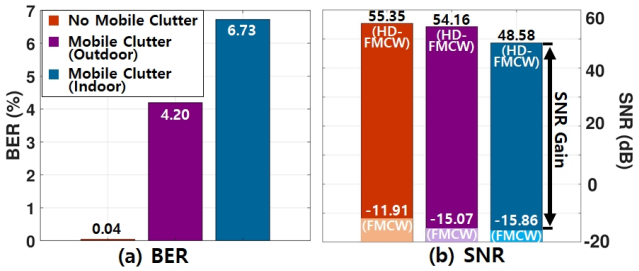

Figure 24: OmniScatter BER and SNR under different mobile clutter scenarios, in comparison to FMCW.

6.7 Mobile Clutter

To verify OmniScatter's robustness under mobile clutter, evaluation under various dynamic background was conducted. Figure 23 depicts the outdoor (roadside) and indoor (cafeteria) experiment scenarios with rich mobile clutters. At roadside (Figure 23(b)), the automobiles were running at the speed limit of 50km/h. The cafeteria experiment (Figure 23(c)) was conducted at lunchtime with 50+ people around. A total of 128 symbols were periodically transmitted for over 10 minutes in order to sufficiently reflect the effect of rich and dynamic mobile clutter. Figure 24(a) showcases that OmniScatter achieves 6.73% BER or lower, where Figure 24(b) exhibits an average SNR of 51.37 dB (i.e., 66.83 dB SNR gain over FMCW) under mobile clutter. We note that the results are comparable to static clutter experiments. This is because, as the distance translates to frequency, the mobile clutter (with dynamic distance) spreads throughout the spectrum and thus its impact is largely amortized. The evaluation demonstrates the practicality of OmniScatter under realistic mobile clutter scenarios.

7 RELATED WORK

mmWave Communication. mmWave communication systems have been discussed for their superior bandwidth over Sub-6 GHz counterparts [32, 50, 65, 76]. Due to significant signal strength degradation, mmWave communication often requires smart tracking of receivers for beam steering [16, 18, 20, 41, 54–56, 66, 67]. On the other hand, the large bandwidth of the mmWave radar facilitates more accurate localization [8, 26, 38, 39, 44, 46]. [7, 11, 34, 52] integrated mmWave communication system with backscatter system, resulting in a low-power and accurate sensing tag platform.

Backscatter Communication. Multiple literature have introduced backscatter to establish an extremely energy-efficient wireless communication links [12, 21, 30, 31, 33, 45, 51, 60, 61, 72, 73, 77, 78], where [57, 62] serve good overviews of recent successes. Meanwhile, papers [24, 29] deployed backscatter tags to enable cross-technology communication. Visible light and acoustic backscatter tags are proposed as substitutes where RF communication is less suitable [15, 25, 59, 64, 68, 69, 71]. Sensitivity of the backscatter tag is one of the principal metrics of the backscatter communication system, where [17, 27, 28, 37, 52, 63, 74] proposed advanced coding schemes for better sensitivity. Other papers sought to increase coverage with smart relays [40, 75], or introduce cross-polarization backscatter tags [42].

CDMA at backscatter [9, 10] offers a robust and concurrent communication system. However, by comparison to the HD-FMCW, the method requires complicated code allocation schemes, especially under network dynamics. OmniScatter avoids coordination complexity associated with code allocation which also offers an advantage in scalability. Furthermore, OmniScatter provides compatibility with the commodity radars for cost-effectiveness and ease of adaptation, as well as extremely lightweight demodulation on top of a simple FFT operation.

8 CONCLUSION

This paper presents OmniScatter, a practical mmWave backscatter system. With the extreme sensitivity of -115 dBm, OmniScatter's theoretical performance is comparable to the widely-deployed 900 MHz RFID. This relieves the necessity of beamforming and alignment, offering agility and robustness to OmniScatter. Further, our unique design of HD-FMCW provides immunity to clutter noise, enabling reliable communication under various practical settings with abundant ambient reflections and blockages. Coordination-free FDMA effortlessly scales to thousands of concurrent tags for further practicality. OmniScatter reader was implemented with commodity radars at 24 GHz and 60 GHz bands, and the tags were prototyped on PCB. Extensive evaluation indicates OmniScatter SNR gain to be above 50 dB, while trace-driven evaluation demonstrates concurrent communication of 1100 tags at BER of ~1.5%.

ACKNOWLEDGMENTS

We thank our shepherd, Prof. Fadel Adib, and the anonymous reviewers for their constructive comments. This work was supported in part by Samsung Research Funding & Incubation Center of Samsung Electronics under Project Number SRFC-IT2101-06, and by the MSIT (Ministry of Science and ICT), Korea, under the ITRC (Information Technology Research Center) support program (IITP-2020-0-01787) supervised by the IITP (Institute of Information & Communications Technology Planning & Evaluation).

REFERENCES

[1] Barton D. K. (ed), "Radars, Volume 3, Pulse Compression", Artech House 1975, 1978.
[2] *Signals & Systems*. McGraw-Hill Education Pvt Limited.
[3] Arduino UNO R3. https://docs.arduino.cc/hardware/uno-rev3.
[4] Atmel 2555 Internal RC Oscillator Calibration for tinyAVR and megaAVR Devices. https://www.microchip.com/en-us/application-notes?rv=1234ab57.
[5] Impinj Speedway RAIN RFID Readers for Flexible Solution Development. https://www.impinj.com/products/readers/impinj-speedway.
[6] Libero SoC v11.8 Archive. https://www.microsemi.com/product-directory/root/5485-libero-soc-v11-8-archive.
[7] M. Alloulah, Z. Radivojevic, R. Mayrhofer, and H. Huang. Kinphy: a kinetic in-band channel for millimetre-wave networks. In *SenSys*, 2019.
[8] R. Ayyalasomayajula, A. Arun, C. Wu, A. Shaikh, S. Rajagopalan, Y. Hu, S. Ganesaraman, C. J. Rossbach, A. Seetharaman, E. Witchel, et al. Locap: Autonomous millimeter accurate mapping of wifi infrastructure. In *NSDI*, 2020.
[9] A. Bletsas, S. Siachalou, and J. N. Sahalos. Anti-collision backscatter sensor networks. *IEEE Transactions on Wireless Communications*, 8(10):5018–5029, 2009.
[10] C. Boyer and S. Roy. Backscatter communication and rfid: Coding, energy, and mimo analysis. *IEEE Transactions on Communications*, 62(3):770–785, 2014.
[11] B. Chen, H. Li, Z. Li, X. Chen, C. Xu, and W. Xu. Thermowave: a new paradigm of wireless passive temperature monitoring via mmwave sensing. In *MobiCom*, 2020.
[12] Z. Chi, X. Liu, W. Wang, Y. Yao, and T. Zhu. Leveraging ambient lte traffic for ubiquitous passive communication. In *SIGCOMM*, 2020.
[13] A. Devices. Eval-tinyrad. https://www.analog.com/en/design-center/evaluation-hardware-and-software/evaluation-boards-kits/eval-tinyrad.html.
[14] H. Friis. A note on a simple transmission formula. *Proceedings of the IRE*, 34(5):254–256, 1946.
[15] R. Ghaffarivardavagh, S. S. Afzal, O. Rodriguez, and F. Adib. Ultra-wideband underwater backscatter via piezoelectric metamaterials. In *SIGCOMM*, 2020.
[16] Y. Ghasempour, M. K. Haider, C. Cordeiro, D. Koutsonikolas, and E. Knightly. Multi-stream beam-training for mmwave mimo networks. In *MobiCom*, 2018.
[17] X. Guo, L. Shangguan, Y. He, J. Zhang, H. Jiang, A. A. Siddiqi, and Y. Liu. Aloba: Rethinking on-off keying modulation for ambient lora backscatter. In *SenSys*, 2020.
[18] M. K. Haider, Y. Ghasempour, D. Koutsonikolas, and E. W. Knightly. Listeer: mmwave beam acquisition and steering by tracking indicator leds on wireless aps. In *MobiCom*, 2018.
[19] F. Harris. On the use of windows for harmonic analysis with the discrete fourier transform. *Proceedings of the IEEE*, 66(1):51–83, 1978.
[20] H. Hassanieh, O. Abari, M. Rodriguez, M. Abdelghany, D. Katabi, and P. Indyk. Fast millimeter wave beam alignment. In *SIGCOMM*, 2018.
[21] M. Hessar, A. Najafi, and S. Gollakota. Netscatter: Enabling large-scale backscatter networks. In *NSDI*, 2019.
[22] Impinj. Rain rfid readers—connectivity devices for enterprise iot solutions. https://www.impinj.com/products/readers.
[23] T. Instruments. Mmwaveicboost. https://www.ti.com/tool/MMWAVEICBOOST.
[24] V. Iyer, V. Talla, B. Kellogg, S. Gollakota, and J. Smith. Inter-technology backscatter: Towards internet connectivity for implanted devices. In *SIGCOMM*, 2016.
[25] J. Jang and F. Adib. Underwater backscatter networking. In *SIGCOMM*. 2019.
[26] C. Jiang, J. Guo, Y. He, M. Jin, S. Li, and Y. Liu. mmvib: micrometer-level vibration measurement with mmwave radar. In *MobiCom*, 2020.
[27] M. Jin, Y. He, X. Meng, D. Fang, and X. Chen. Parallel backscatter in the wild: When burstiness and randomness play with you. In *MobiCom*, 2018.
[28] M. Jin, Y. He, X. Meng, Y. Zheng, D. Fang, and X. Chen. Fliptracer: Practical parallel decoding for backscatter communication. *IEEE/ACM Transactions on Networking*, 27(1):330–343, 2019.
[29] J. Jung, J. Ryoo, Y. Yi, and S. M. Kim. Gateway over the air: towards pervasive internet connectivity for commodity iot. In *MobiSys*, 2020.
[30] B. Kellogg, V. Talla, S. Gollakota, and J. R. Smith. Passive wi-fi: Bringing low power to wi-fi transmissions. In *NSDI*, 2016.
[31] B. Kempke, P. Pannuto, B. Campbell, and P. Dutta. Surepoint: Exploiting ultra wideband flooding and diversity to provide robust, scalable, high-fidelity indoor localization. In *SenSys*, 2016.
[32] J. O. Lacruz, D. Garcia, P. J. Mateo, J. Palacios, and J. Widmer. mm-flex: an open platform for millimeter-wave mobile full-bandwidth experimentation. In *MobiSys*, 2020.
[33] A. Lazaro, M. Lazaro, R. Villarino, D. Girbau, and P. de Paco. Car2car communication using a modulated backscatter and automotive fmcw radar. *Sensors*, 2021.
[34] Z. Li, B. Chen, Z. Yang, H. Li, C. Xu, X. Chen, K. Wang, and W. Xu. Ferrotag: A paper-based mmwave-scannable tagging infrastructure. In *SenSys*, 2019.
[35] Z. Li and T. He. Webee: Physical-layer cross-technology communication via emulation. In *MobiCom*, 2017.
[36] X. Liu, Z. Chi, W. Wang, Y. Yao, P. Hao, and T. Zhu. Verification and redesign of OFDM backscatter. In *NSDI*, 2021.
[37] X. Liu, Z. Chi, W. Wang, Y. Yao, and T. Zhu. Vmscatter: A versatile mimo backscatter. In *NSDI*, 2020.
[38] C. X. Lu, S. Rosa, P. Zhao, B. Wang, C. Chen, J. A. Stankovic, N. Trigoni, and A. Markham. See through smoke: robust indoor mapping with low-cost mmwave radar. In *MobiSys*, 2020.
[39] C. X. Lu, M. R. U. Saputra, P. Zhao, Y. Almalioglu, P. P. de Gusmao, C. Chen, K. Sun, N. Trigoni, and A. Markham. milliego: single-chip mmwave radar aided egomotion estimation via deep sensor fusion. In *SenSys*, 2020.
[40] Y. Ma, N. Selby, and F. Adib. Drone relays for battery-free networks. In *SIGCOMM*, 2017.
[41] M. H. Mazaheri, S. Ameli, A. Abedi, and O. Abari. A millimeter wave network for billions of things. In *SIGCOMM*. 2019.
[42] M. H. Mazaheri, A. Chen, and O. Abari. mmtag: a millimeter wave backscatter network. In *SIGCOMM*, 2021.
[43] P. Nikitin, K. Rao, S. Lam, V. Pillai, R. Martinez, and H. Heinrich. Power reflection coefficient analysis for complex impedances in rfid tag design. *IEEE Transactions on Microwave Theory and Techniques*, 53(9):2721–2725, 2005.
[44] I. Pefkianakis and K.-H. Kim. Accurate 3d localization for 60 ghz networks. In *SenSys*, 2018.
[45] Y. Peng, L. Shangguan, Y. Hu, Y. Qian, X. Lin, X. Chen, D. Fang, and K. Jamieson. Plora: A passive long-range data network from ambient lora transmissions. In *SIGCOMM*, 2018.
[46] A. Prabhakara, V. Singh, S. Kumar, and A. Rowe. Osprey: a mmwave approach to tire wear sensing. In *MobiSys*, 2020.
[47] S. Research. The next hyper-connected experience for all. Technical report, Samsung, 2020.
[48] T. I. Sandeep Rao. Introduction to mmwave sensing: Fmcw radars. https://training.ti.com/node/1139153.
[49] L. Shangguan and K. Jamieson. The design and implementation of a mobile rfid tag sorting robot. In *MobiSys*, 2016.
[50] V. Singh, S. Mondal, A. Gadre, M. Srivastava, J. Paramesh, and S. Kumar. Millimeter-wave full duplex radios. In *MobiCom*, 2020.
[51] E. Soltanaghaei, A. Dongare, A. Prabhakara, S. Kumar, A. Rowe, and K. Whitehouse. Tagfi: Locating ultra-low power wifi tags using unmodified wifi infrastructure. *IMWUT*, 2021.
[52] E. Soltanaghaei, A. Prabhakara, A. Balanuta, M. Anderson, J. M. Rabaey, S. Kumar, and A. Rowe. Millimetro: mmwave retro-reflective tags for accurate, long range localization. In *MobiCom*, 2021.
[53] P. Sparks. The route to a trillion devices. 2017.
[54] S. Sur, I. Pefkianakis, X. Zhang, and K.-H. Kim. Wifi-assisted 60 ghz wireless networks. In *MobiCom*, 2017.
[55] S. Sur, I. Pefkianakis, X. Zhang, and K.-H. Kim. Towards scalable and ubiquitous millimeter-wave wireless networks. In *MobiCom*, 2018.
[56] S. Sur, X. Zhang, P. Ramanathan, and R. Chandra. Beamspy: Enabling robust 60 ghz links under blockage. In *NSDI*, 2016.
[57] V. Talla, J. Smith, and S. Gollakota. Advances and open problems in backscatter networking. *GetMobile*, 2021.
[58] I. Technologies. Demo distance2go. https://www.infineon.com/cms/en/product/evaluation-boards/demo-distance2go/.
[59] F. Tonolini and F. Adib. Networking across boundaries: enabling wireless communication through the water-air interface. In *SIGCOMM*, 2018.
[60] A. Varshney, O. Harms, C. Pérez-Penichet, C. Rohner, F. Hermans, and T. Voigt. Lorea: A backscatter architecture that achieves a long communication range. In *SenSys*, 2017.
[61] A. Wang, V. Iyer, V. Talla, J. R. Smith, and S. Gollakota. Fm backscatter: Enabling connected cities and smart fabrics. In *NSDI*, 2017.
[62] J. Wang, L. Chang, O. Abari, and S. Keshav. Are rfid sensing systems ready for the real world? In *MobiSys*, 2019.
[63] J. Wang, J. Zhang, R. Saha, H. Jin, and S. Kumar. Pushing the range limits of commercial passive rfids. In *NSDI*, 2019.
[64] P. Wang, L. Feng, G. Chen, C. Xu, Y. Wu, K. Xu, G. Shen, K. Du, G. Huang, and X. Liu. Renovating road signs for infrastructure-to-vehicle networking: A visible light backscatter communication and networking approach. In *MobiCom*, 2020.
[65] S. Wang, J. Huang, and X. Zhang. Demystifying millimeter-wave v2x: Towards robust and efficient directional connectivity under high mobility. In *MobiCom*, 2020.
[66] T. Wei and X. Zhang. Pose information assisted 60 ghz networks: Towards seamless coverage and mobility support. In *MobiCom*, 2017.
[67] T. Wei, A. Zhou, and X. Zhang. Facilitating robust 60 ghz network deployment by sensing ambient reflectors. In *NSDI*, 2017.
[68] Y. Wu, P. Wang, and C. Xu. Improving visible light backscatter communication with delayed superimposition modulation. In *MobiCom*, 2019.
[69] Y. Wu, P. Wang, K. Xu, L. Feng, and C. Xu. Turboboosting visible light backscatter communication. In *SIGCOMM*, 2020.
[70] Y. Xing, O. Kanhere, S. Ju, and T. Rappaport. Indoor wireless channel properties at millimeter wave and sub-terahertz frequencies. pages 1–6, 12 2019.
[71] X. Xu, Y. Shen, J. Yang, C. Xu, G. Shen, G. Chen, and Y. Ni. Passivevlc: Enabling practical visible light backscatter communication for battery-free iot applications. In *MobiCom*, 2017.

[72] P. Zhang, D. Bharadia, K. Joshi, and S. Katti. Hitchhike: Practical backscatter using commodity wifi. In *SenSys*, 2016.
[73] P. Zhang, M. Rostami, P. Hu, and D. Ganesan. Enabling practical backscatter communication for on-body sensors. In *SIGCOMM*, 2016.
[74] J. Zhao, W. Gong, and J. Liu. Spatial stream backscatter using commodity wifi. In *MobiSys*, 2018.
[75] J. Zhao, W. Gong, and J. Liu. Towards scalable backscatter sensor mesh with decodable relay and distributed excitation. In *MobiSys*, 2020.
[76] R. Zhao, T. Woodford, T. Wei, K. Qian, and X. Zhang. M-cube: A millimeter-wave massive mimo software radio. In *MobiCom*, 2020.
[77] R. Zhao, F. Zhu, Y. Feng, S. Peng, X. Tian, H. Yu, and X. Wang. Ofdma-enabled wi-fi backscatter. In *MobiCom*, 2019.
[78] F. Zhu, Y. Feng, Q. Li, X. Tian, and X. Wang. Digiscatter: efficiently prototyping large-scale ofdma backscatter networks. In *MobiSys*, 2020.